

Gate-tuned high frequency response of carbon nanotube Josephson junctions

J.-P. Cleuziou¹, W. Wernsdorfer², S. Andergassen², S.
Florens², V. Bouchiat², Th. Ondarcuhu¹, M. Monthieux¹

¹*CEMES-CNRS, BP 94347, 31055 Toulouse Cedex 4, France*

²*Institut Néel, CNRS/UJF, BP 166, 38042 Grenoble Cedex 9, France*

(Dated: April 20, 2007)

Abstract

Carbon nanotube (CNT) Josephson junctions in the open quantum dot limit exhibit superconducting switching currents which can be controlled with a gate electrode. Shapiro voltage steps can be observed under radiofrequency current excitations, with a damping of the phase dynamics that strongly depends on the gate voltage. These measurements are described by a standard RCSJ model showing that the switching currents from the superconducting to the normal state are close to the critical current of the junction. The effective dynamical capacitance of the nanotube junction is found to be strongly gate-dependent, suggesting a diffusive contact of the nanotube.

PACS numbers: 74.50.+r, 74.45.+c, 73.63.Kv, 73.63.Fg

It was recently demonstrated that carbon nanotube (CNT) weak links, connecting two superconducting leads [1], can be gate-controlled Josephson junctions [2, 3, 4, 5, 6, 7, 8] and even gate-controlled π -junctions [6]. The first interesting application of CNT Josephson junctions are superconducting transistors [4, 5] and superconducting quantum interference devices (SQUIDs) [6], which are promising candidates for the detection of individual magnetic molecules. They might also prove useful as building blocks for more complicated superconducting devices [9] and new readout schemes [10, 11].

For all these devices, the critical current I_c and the high frequency response of CNT Josephson junctions plays an important role, which is studied in this letter. Indeed, previous investigations showed that the magnitude of the switching current I_{sw} of such CNT devices appeared to be very different from theoretical predictions: in the first experiments it was observed to be 10 times larger [1] and later 10 times smaller [4, 5, 6, 7, 8] than the result of Ambegaokar and Baratoff [12], reformulated for a quantum dot (QD) in [13]. Moreover, all these previous measurements were performed for a static bias, without retrieving the effect of radiofrequency (RF) irradiation.

The electronic transport through a CNT junction can be described by a QD in between two conducting leads. The energy level spacing ΔE depends on the length of the junction and the nature of the conducting leads. The transport can be classified into three limits depending on the ratio between the transparency Γ of the QD barriers and the charging energy U [14]: (i) for $h\Gamma \ll U$, the maximum conductance at zero bias obeys $G_{\max} \ll 2e^2/h$. In this so-called closed QD regime the charging effects dominate the transport characterized by well-resolved Coulomb blockade diamonds [15]. (ii) for $h\Gamma \approx U$ holds $e^2/h \lesssim G_{\max} \lesssim 2e^2/h$. In this intermediate transparency regime charging effects as well as higher-order tunneling processes are very important. Here, transport measurements show that Coulomb blockade diamonds, corresponding to an odd number of electrons, are connected by Kondo ridges [2, 16]. For superconducting leads, higher-order multiple Andreev reflections (MARs) are well resolved [3, 4]. (iii) For $h\Gamma \gg U$, the conductance is close to $4e^2/h$ and corresponds to the open QD regime (the factor 4 reflects the two modes of the CNT band structure as well as the two spin orientations), where Coulomb blockade diamonds are not observed. This leads to a relatively high supercurrent for all gate voltages. Gate-modulated Fabry-Perot interferences can be observed in the last two regimes [17].

An important advantage of these devices is that backgate and sidegate electrodes can

be used to vary both Γ and the energy levels position in the nanotube, thus permitting to change the electric transport regime [18]. This tunability allowed us in a previous study to capture both Kondo screened and unscreened junctions, leading to the observation of a $0-\pi$ transition [6]. Similarly, we found that the QD barrier can be varied with the thickness of the Pd contacts, enabling to access also all three transport regimes.

Previous measurements on CNT Josephson junctions were in the intermediated or closed QD regime [19]. Here we present the first measurements in the open QD regime using a Pd thickness of 7 nm. The present description concentrates on a single device, similar data were however obtained on a couple of other devices fabricated on the same chip.

The CNT Josephson junction were fabricated as presented earlier [6]. We started from a degenerately n-doped silicon substrate with 350 nm thick thermally grown SiO_2 layer on top used as a backgate. Single-walled CNTs were deposited using a combing technique [20]. The nanotube location was imaged by atomic force microscopy (AFM) and aligned e-beam lithography patterned the contacts [21]. The length of the tube section between the contacts was about 200 nm. Metal electrodes consisting of a thickness of 3 to 7 nm of Pd followed by 50 nm of Al, were deposited using electron-gun evaporation. Pd provides high-transparency contacts to the carbon nanotubes. Al is a superconductor having a critical temperature of about 1.2 K. The room temperature resistance varied between 10 and 60 k Ω , strongly depending on the thickness of Pd. Only devices with no significant gate effect at room temperature were used for our studies. We found that for Pd thicknesses below about 3 nm, the CNT junction was in the closed QD regime, for 4 to 6 nm in the intermediate, and for 7 nm and more in the open QD regime.

The measurements were performed in a shielded cryostat having heavily filtered lines in order to minimize the electronic noise reaching the sample, since electronic noise can reduce and even suppress the switching current of the CNT-SQUID. Our home-built filtering system was presented in [6]. We used mainly a four-probe, current-biased method. with a bias resistance of about 65 M Ω at 4.5 K and voltage dividers at room temperature. The voltage signal of the sample was first pre-amplified by a factor of 10^4 and then measured using an oscilloscope or a lock-in amplifier. High frequency ac current modulations in the frequency range between 1 and 12 GHz were induced via an inductive coupling.

The effective BCS gap Δ_{eff} of the superconducting leads felt by the CNT was estimated by voltage versus current measurements as a function of temperature. We found a transition

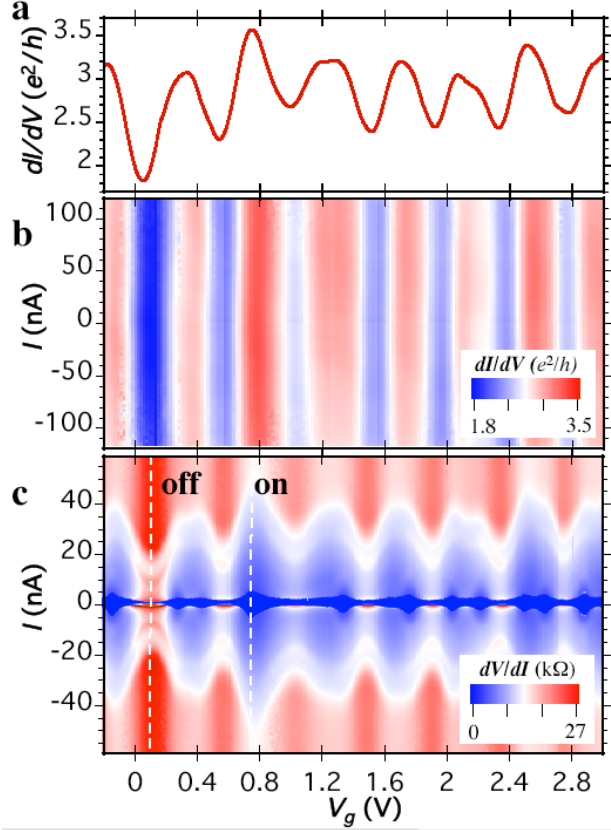


FIG. 1: (Color online) Electric transport through a CNT junction as a function of gate-voltage V_g . (a) Differential conductivity dI/dV versus V_g at zero bias. (b) dI/dV -map versus current bias I_{sd} and V_g in the normal state ($H_z = 50$ mT). (c) Differential resistivity dV/dI -map versus I_{sd} and V_g in the superconducting state ($H_z = 0$). The dotted lines indicates the off-state and on-state, which are further studied in Figs. 2 to 4.

temperature $T_c = 0.7$ K, yielding a $\Delta_{\text{eff}} = 1.76 k_B T_c = 0.1$ meV. The energy level spacing of the CNT were determined ~ 10 meV [6]. However, due to the high transparency of the contacts the effect of the Coulomb energy is much smaller here.

In Fig. 1a and 1b, a magnetic field of $H_z = 50$ mT was applied perpendicular to the electrode plane in order to suppress the superconductivity of the leads. The differential conductivity dI/dV is plotted versus gate voltage at zero bias in Fig. 1a and, in addition, as a function of source-drain current I_{sd} in Fig. 1b. dI/dV oscillates between about 1.8 and $3.5 e^2/h$ and is I_{sd} -independent in the considered range. dI/dV is maximal when a quantum level of the CNT is aligned with respect to the Fermi energy of the leads. A current can

then flow by resonant tunneling through the CNT, and we denominate this regime as an on-state. When the quantum levels are far from the Fermi energy, the current is reduced (off-state). This CNT junction is clearly in the open QD regime because the reduction is only about a factor of two and Coulomb blockade effects are not directly observable.

Fig. 1c presents the same measurements as in Fig. 1b but with superconducting leads ($H_z = 0$). Because dI/dV diverges, the differential resistivity dV/dI is plotted. For small I_{sd} a supercurrent is observed, which is evidenced by a nearly zero-resistance state. At a certain bias current denoted by switching current I_{sw} , the junction switches from the superconducting to the normal state. I_{sw} is strongly gate-voltage dependent: it is maximal (minimal) in the on-state (off-state). Most of the on-states are split into two I_{sw} maxima suggesting that there is still a small influence of Coulomb interaction. Note that higher-order MARs are not observed, which is probably due to strong broadening effects induced by the high transparency contacts.

Fig. 2a and 2b show typical voltage versus current curves at several temperatures for the on- and off-state. The on-state is characterized by the largest I_{sw} and small hysteresis effects, that is the retrapping current is close to I_{sw} . Furthermore, dV/dI increase for $I_{sd} > I_{sw}$ in the considered range. In the off-state, the hysteresis effects are very large and dV/dI decrease for $I_{sd} > I_{sw}$. A small temperature-dependent resistance is observed at zero-bias, which is mainly due to temperature-induced phase diffusion [22].

The high frequency response of the CNT junctions is examined by voltage-current curves in the presence of RF-fields. Figs. 3a and 4a show the appearance of constant voltage Shapiro steps, which are due to the harmonical synchronization of the Josephson oscillations and the applied RF excitations. The steps appear at voltages equal to $nf\phi_0$ where $n = 1, 2, \dots$ and ϕ_0 is a flux quanta. We checked this linear relation in the frequency range between $f = 1$ to 15 GHz (data not shown). The influence of the RF current I_{RF} on the Shapiro steps is presented on Figs. 3b and 4b for the on- and off-state, respectively. The plots show the differential resistance as a function of I_{RF} and I_{sd} , giving rise to a complicated pattern of non-dissipative lobes.

We modelled the data with a phenomenological description of time-dependent transport in superconducting junctions based on both the standard Josephson relations and on classical circuit theory, the so-called resistively and capacitively shunted junction (RCSJ) model [23, 24]. This invokes simple differential equations that govern the dynamics of the phase ϕ

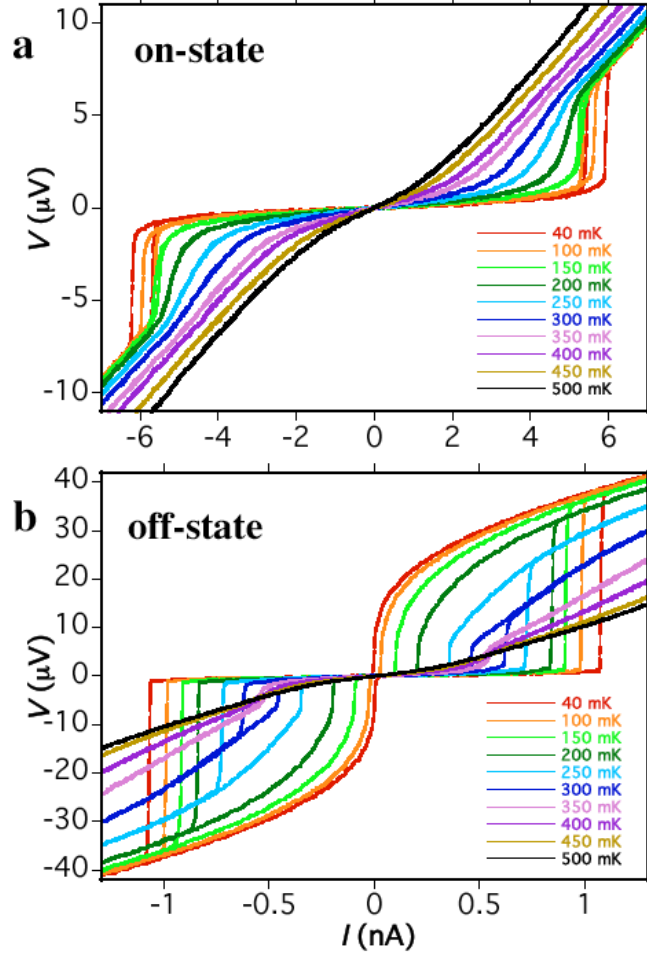


FIG. 2: (Color online) Voltage versus current characteristics for a CNT junction in (a) the on-state and (b) off-state at several temperatures. (a) and (b) correspond to maximal and minimal switching currents in Fig. 1c, respectively. The current was swept at the sweep rates of 5 and 0.2 nA/s for (a) and (b), respectively. Note that each curve is a single sweep (no data averaging was performed) and the slope at the switching currents was limited by the filtering.

across the junction:

$$\hbar \frac{d\phi}{dt} = 2eV \quad (1a)$$

$$I(t) = C \frac{dV}{dt} + I_{qp}(V) + I_c \sin \phi, \quad (1b)$$

where V is the instantaneous voltage drop, $I(t) = I_{sd} + I_{RF} \sin(\omega t)$ the injected current with an oscillating part at the radiofrequency $f = \omega/2\pi$, $I_{qp}(V)$ the quasiparticle contribution to the current, I_c the critical supercurrent, and C the capacitance of the junction.

Assuming an ohmic quasiparticle current $I_{\text{qp}} = V/R$ and defining a basic frequency scale $\gamma = 2eRI_c/\hbar$, one obtains two relevant dimensionless parameters in the analysis of the Shapiro steps: i) the reduced pulsation $\tilde{\omega} = \omega/\gamma$ characterizing the shape of the Shapiro steps [25, 26] (pure Bessel functions are obtained in the limit $\tilde{\omega} \gg 1$ only); ii) the quality factor $Q = \sqrt{\gamma RC}$ that controls the damping of the phase dynamics.

The parameters are adjusted to the experimental data in the RF driven regime where the dynamics is less sensitive to phase diffusion [22]. The analysis of the experimental data in the on-state reveals a globally good agreement for $Q \lesssim 1$, i.e. the RSJ model with no capacitance. Indeed, the geometrical capacitance of CNT junctions is very small (~ 30 aF). This finding is supported by the small hysteresis effects of the VI -curves (Fig. 2a). Note that the predicted I_c is very close to I_{sw} at $I_{\text{RF}} = 0$. The Shapiro step positions present however small but appreciable deviations to the pure Bessel functions. Their precise shape can indeed be more accurately described using a reduced pulsation $\tilde{\omega} \sim 0.35$. Furthermore, a clear downward dispersion of the lobes is observed, which may be attributed to the non-ohmic character of the quasiparticle current $I_{\text{qp}}(V)$ above the threshold I_{sw} . Simulations of the phase dynamics with such non-linear RSJ model, where the non-linear R from the VI -curves in the resistive state of Fig. 2 was included, are provided in Fig. 3c and compare favorably to the experimental data.

Regarding the off-state, several issues point to additional underdamping effects: the VI -curves are strongly hysteretic and the degree of hysteresis diminishes with increasing temperature (Fig. 2b) [24]. Moreover, the low-bias Shapiro steps present a peculiar threshold behavior (Fig. 4b), while the lobes show an upward dispersion. These properties can not be explained within the usual RCSJ model, and may be only accounted for at a qualitative level by introducing a rather large effective capacitance $C \approx 1$ fF and a non-linear quasiparticle resistance (stronger than in the on-state discussed above). Fig. 4c shows a partial agreement between our simulations and the data. The gate-dependence of C suggests a diffusive CNT contact in the off-state, i.e. additional capacities coming from the CNT contacts. Indeed, for the off state, the electrode/nanotube capacitance has to be taken into account since the Pd/nanotube contact is known to be distributed over a larger part of the contact [27]. Its value can be rather strong (~ 1 fF). For the on-state however, the capacitance of the contact can be strongly renormalized by the tunnel effect [28] and the capacitance of the junction is mainly due to the nanotube self-capacitance estimated as 30 aF for a nanotube portion of

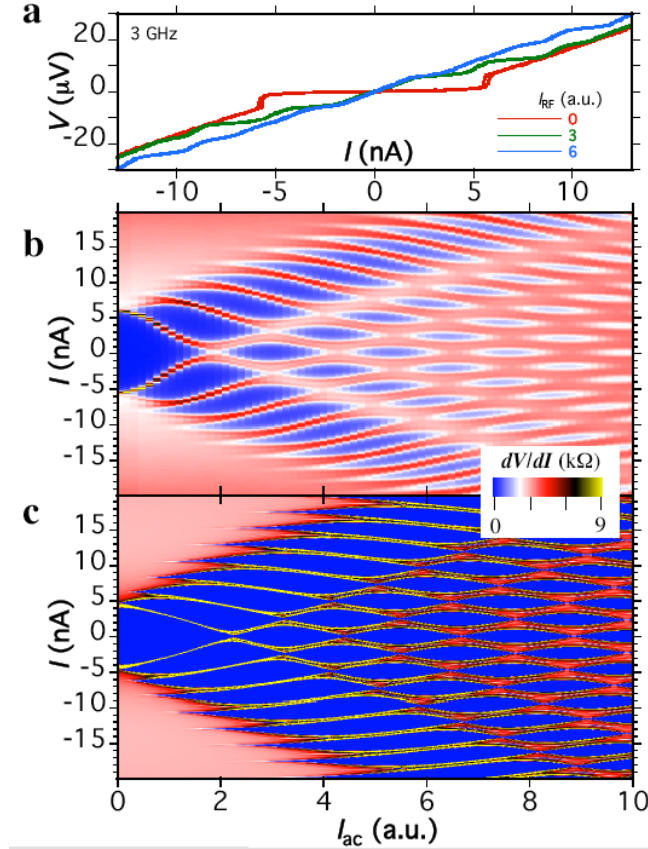


FIG. 3: (Color online) RF response in the on-state. (a) Voltage versus current characteristics at several RF amplitudes I_{RF} . (b) Differential resistance dI/dV -maps versus I_{sd} and I_{RF} for $f = 3$ GHz. (c) Simulation of the data in (b) using the non-linear RSJ model.

200 nm [29]. A more thorough analysis of quantum and thermal fluctuation effects on the Shapiro steps in the spirit of references [30, 31] is clearly beyond the scope of the present study. We point out however that these effects probably do not account for the strong reduction of the critical current, as the above analysis demonstrated in the on-state.

In conclusion, we studied the critical currents and the constant-voltage Shapiro steps under RF irradiation of a strongly coupled CNT Josephson junction, and discovered a strong gate-voltage dependence. These junctions are therefore very promising as tunable RF building blocks for superconducting devices.

This work was partially supported by the CNRS ACI NOCIEL and ANR QuSpins programs. Clean room processes were supported by the CNRS RTB program using the technological facilities of the Laboratory for Analysis and Architecture of Systems (University of

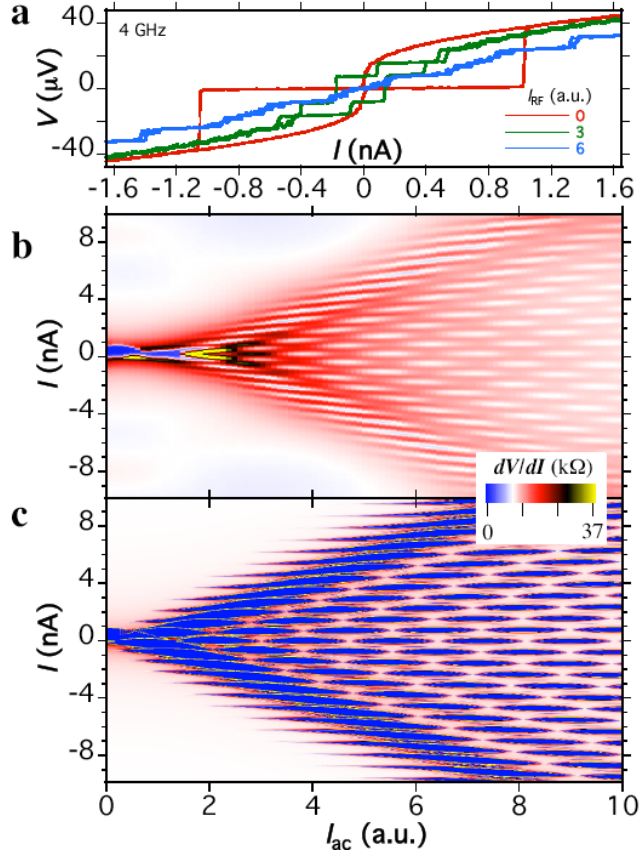


FIG. 4: (Color online) RF response in the off-state. (a) VI -characteristics at several I_{RF} . (b) dI/dV -maps versus I_{sd} and I_{RF} for $f = 4$ GHz. (c) Simulation of the data in (b) using the non-linear RCSJ model.

Toulouse - France). We thanks F. Balestro, O. Buisson, F. Carcenac, J. Clarke, E. Eyraud, D. Feinberg, and I. Siddiqi for valuable contributions and helpful discussions.

-
- [1] A. Y. Kasumov and et al., *Science* **397**, 598 (1999).
 - [2] M. R. Buitelaar, T. Nussbaumer, and C. Schonenberger, *Phys. Rev. Lett.* **89**, 256801 (2002).
 - [3] M. R. Buitelaar, W. Belzig, T. Nussbaumer, B. Babic, C. Bruder, and C. Schonenberger, *Phys. Rev. Lett.* **91**, 057005 (2003).
 - [4] P. Jarillo-Herrero, J.A. van Dam, and L.P. Kouwenhoven, *Nature* **439**, 953 (2006).
 - [5] H. I. Jorgensen, K. Grove-Rasmussen, T. Novotny, K. Flensberg, and P. E. Lindelof, *Phys. Rev. Lett.* **96**, 207003 (2006).

- [6] J.-P. Cleuziou, W. Wernsdorfer, V. Bouchiat, Th. Ondarcuhu, and M. Monthieux, *Nature Nanotech.* **1**, 53 (2006).
- [7] T. Tsuneta, L. Lechner, and P. J. Hakonen, *Phys. Rev. Lett.* **98**, 087002 (2007).
- [8] A. Eichler, M. Weiss, S. Oberholzer, C. Schonberger, A. Levy Yeyati, and J. C. Cuevas, *cond-mat/0703082*.
- [9] I. Chiorescu, Y. Nakamura, C.J.P.M. Harmans, and J.E. Mooij, *Science* **299**, 1869 (2003).
- [10] I. Siddiqi, R. Vijay, F. Pierre, C. M. Wilson, M. Metcalfe, C. Rigetti, L. Frunzio, and M. H. Devoret, *Phys. Rev. Lett.* **93**, 207002 (2004).
- [11] I. Siddiqi, R. Vijay, F. Pierre, C. M. Wilson, L. Frunzio, M. Metcalfe, C. Rigetti, R. J. Schoelkopf, M. H. Devoret, D. Vion, and D. Esteve, *Phys. Rev. Lett.* **94**, 027005 (2005).
- [12] V. Ambegaokar and A. Baratoff, *Phys. Rev. Lett.* **10**, 486 (1963).
- [13] C. W. J. Beenakker and H. van Houten, in *see also condmat/0111505*, edited by H. Koch and H. Luebbig (Springer, Berlin, 1992), pp. 175–179.
- [14] For short CNT junction of few 100 nm, $\Delta E > h\Gamma, U$.
- [15] D. H. Cobden and J. Nygard, *Phys. Rev. Lett.* **89**, 046803 (2002).
- [16] D. Goldhaber-Gordon, J. Gores, M. A. Kastner, Hadas Shtrikman, D. Mahalu, and U. Meirav, *Phys. Rev. Lett.* **81**, 5225 (1998).
- [17] W.J. Liang and et al., *Nature* **411**, 665 (2001).
- [18] J.-P. Cleuziou, W. Wernsdorfer, V. Bouchiat, Th. Ondarcuhu, and M. Monthieux, *cond-mat/0610622*.
- [19] The data in [4] were interpreted to be in the open QD regime. However, we think that the well-resolved higher-order MAR fine-structures as well as the high resistivity in the off-states suggest that these devices operated in the intermediate transport regime. The observation of $G_{\max} \approx 4e^2/h$ could be explained by the large CNT diameter of 4 to 7 nm and the observation of Fano resonances suggesting that the junction was not made out of an individual single-walled CNT.
- [20] S. Gerdes, T. Ondarcuhu, S. Cholet, and C. Joachim, *EuroPhys. Lett.* **48**, 292 (1999).
- [21] M. Sagnes, J.M. Broto, B. Raquet, T. Ondarcuhu, C. Laurent, E. Flahaut, C. Vieu, and F. Carcenac, *Microelec. Eng.* **67**, 683 (2003).
- [22] D. Vion, M. Gotz, P. Joyez, D. Esteve, and M.H. Devoret, *Phys. Rev. Lett.* **77**, 3435 (1996).
- [23] A. Barone and G. Paterno, *Physics and Applications of the Josephson effect* (John Wiley and

- Sons, New York, 1982), Vol. 1.
- [24] M. Tinkham, *Introduction to Superconductivity*, 2 ed. (McGraw-Hill, New York, 1996), Vol. 1.
- [25] K. K. Likharev and V. K. Semenov, *Radiotech. Elektron.* **16**, 2167 (1971).
- [26] P. Russer, *J. Appl. Phys.* **43**, 2008 (1972).
- [27] N. Nemeč, D. Tomanek, and G. Cuniberti, *Phys. Rev. Lett.* **96**, 076802 (2006).
- [28] K. Flensberg, *Phys. Rev. B* **48**, 11156 (1993).
- [29] Note that in the on-state we neglected the quantum capacitance of the nanotube, which is estimated ~ 100 aF. See also S. Rosenblatt *et al.*, *Nano Lett.* **2**, 869 (2002), and S. Ilani, L. A. K. Donev, M. Kindermann and P. L. McEuen, *Nature Physics* **2**, 687 (2006).
- [30] Y. M. Ivanchenko and L. A. Zilberman, *Sov. Phys. JETP.* **28**, 1272 (1969).
- [31] Raphael Duprat and Alfredo Levy Yeyati, *Phys. Rev. B* **71**, 054510 (2005).

ANNEX

We present here additional data measured at different temperatures and microwave frequencies. Fig. 5 shows differential resistance maps for the on-state at several temperature. Although the Shapiro steps are blurred because of phase diffusion induced by the temperature, the step positions are nearly temperature independent.

The frequency dependence of the pattern of non-dissipative lobes is present in the differential resistance maps of Figs. 6 and 7 for the on-state and off-state, respectively.

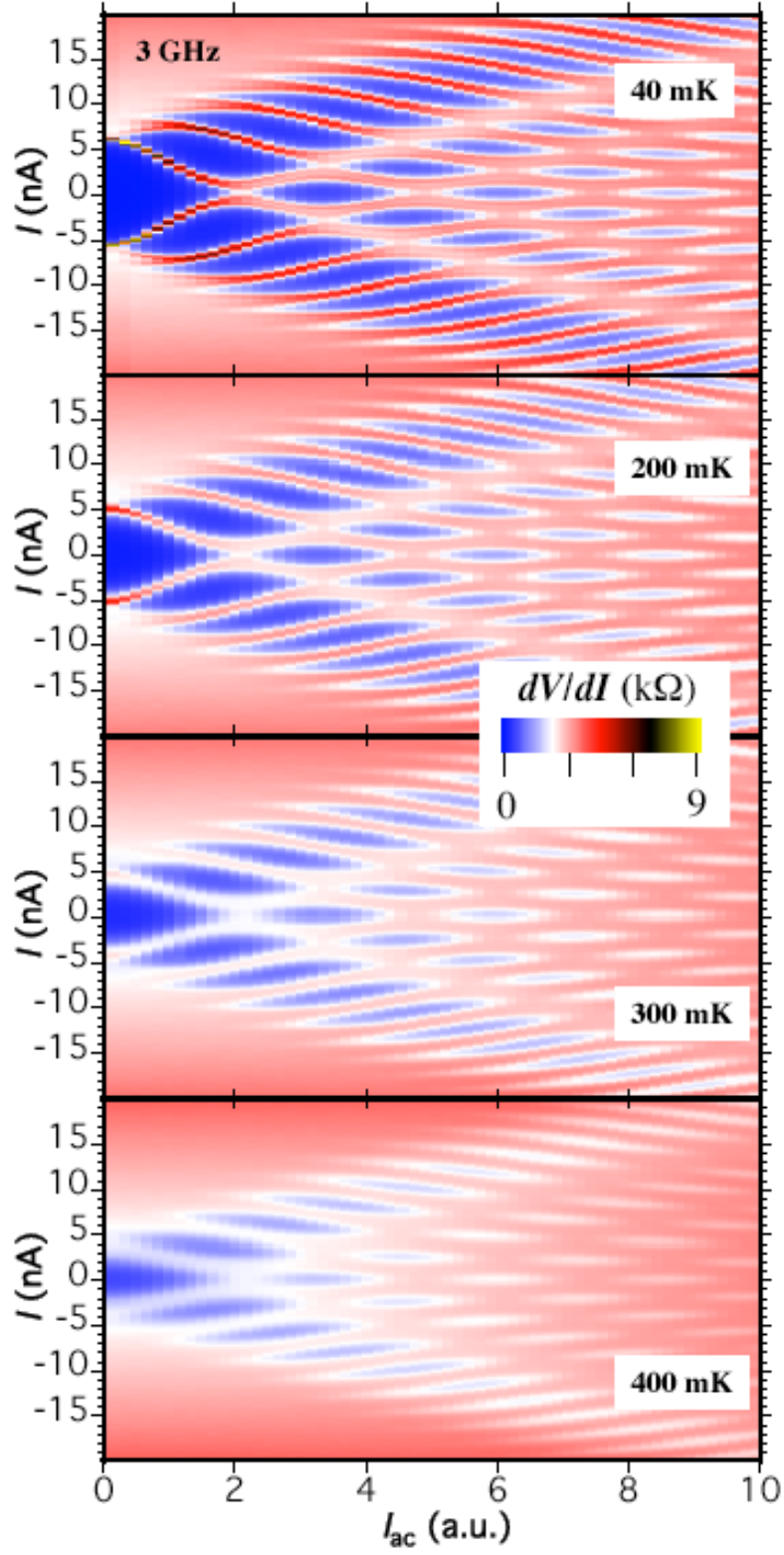


FIG. 5: (Color online) RF response in the on-state at four different temperatures. dI/dV -maps versus I_{sd} and I_{RF} are displayed for $f = 3$ GHz.

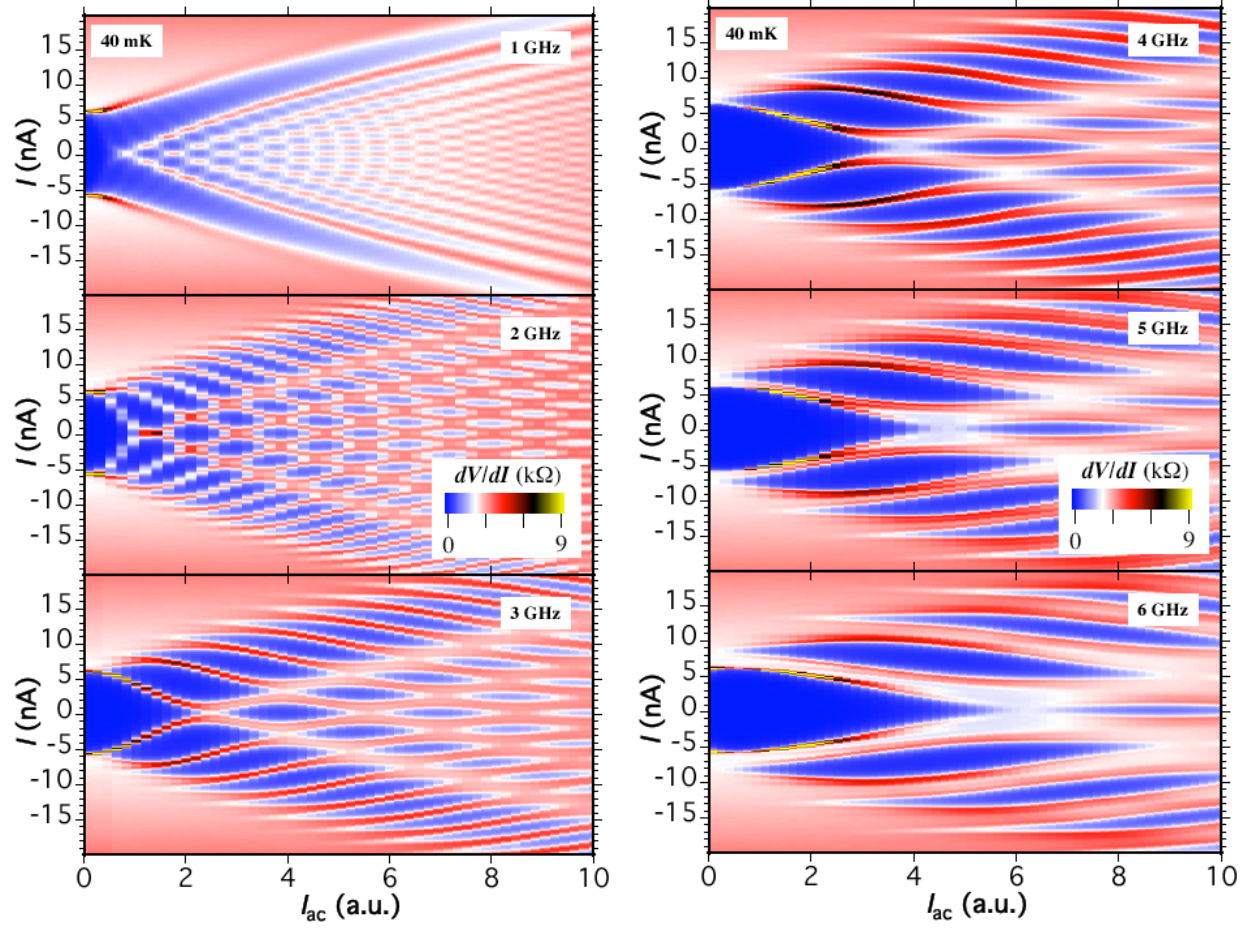


FIG. 6: (Color online) RF response in the on-state at different microwave frequencies. dI/dV -maps versus I_{sd} and I_{RF} are displayed for 40 mK.

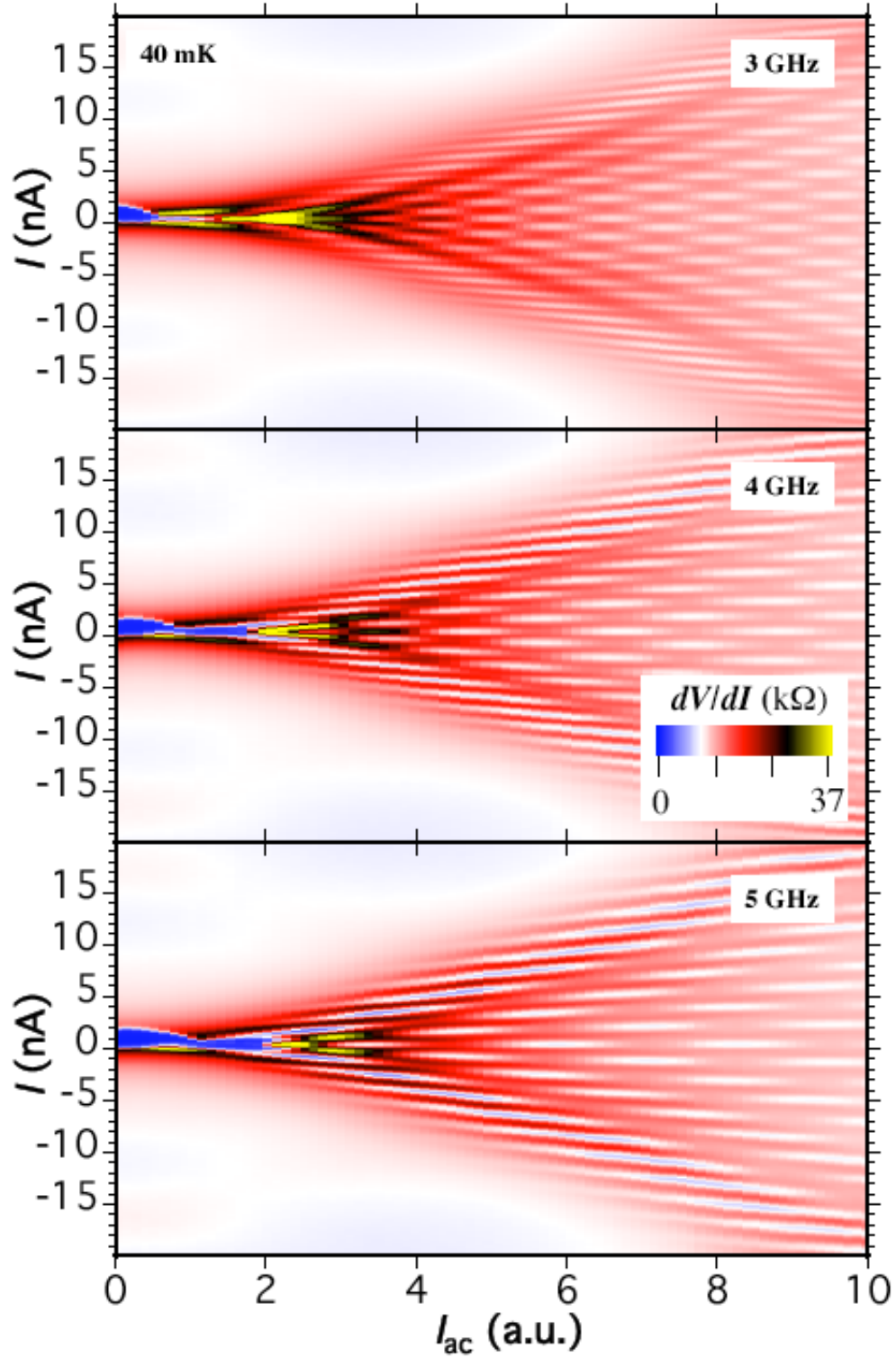


FIG. 7: (Color online) RF response in the off-state at different microwave frequencies. dI/dV -maps versus I_{sd} and I_{RF} are displayed for 40 mK.